Shallow Sea-Floor Reflectance and Water Depth Derived by Unmixing Multispectral Imagery*

Abstract

A major problem for mapping shallow water zones by the analysis of remotely sensed data is that contrast effects due to water depth obscure and distort the special nature of the substrate. This paper outlines a new method which unmixes the exponential influence of depth in each pixel by employing a mathematical constraint. This leaves a multispectral residual which represents relative substrate reflectance. Input to the process are the raw multispectral data and water attenuation coefficients derived by the co-analysis of known bathymetry and remotely sensed data. Outputs are substrate-reflectance images corresponding to the input bands and a greyscale depth image. The method has been applied in the analysis of Landstat TM data at Hamelin Pool in Shark Bay, Western Australia. Algorithm derived substrate reflectance images for Landsat TM bands 1, 2, and 3 combined in color represent the optimum enhancement for mapping or classifying substrate types. As a result, this color image successfully delineated features, which were obscured in the raw data, such as the distributions of sea-grasses, microbial mats, and sandy area.

Introduction

Multispectral scanners, mounted on aircraft and satellites, are valuable tools for mapping the Earth's surface. Passive sensors such as the Lansat Thematic Mapper (TM) measure reflected radiation from visible and infrared ranges of the solar spectrum. Many investigators have shown the value of applying satellite scanner data to mapping the shallow water environment, particularly utilizing the visible wavelengths which penetrate to greater water depths (Smith and Baker, 1981).

A common mapping technique is to perform a classification on the multispectral data to show substrate types. The major problem with classification of raw digital numbers (DNs) is that variations in water depth may alter the spectral characteristics of the substrate. The aim of this paper is to outline all the effects which contribute to the raw satellite DN value and, with this understanding, derive an algorithm which allows the mapping of the spectral characteristics of substrate materials free from the confusing influence of depth.

The situation is complex because radiation must pass through two media–atmosphere and water–before interacting with the substrate and again traversing the same media (see Figure 1). Also, atmospheric back-scatter and background water surface reflectance may add to the signal. Assuming that it is possible to look at only the signal emerging from the water mass, we must deal with a complex optical interaction of parameters which include.

- substrate reflectance,
- water depth, and
- material in the water column [e.g., organic matter, suspended sediments, and dissolved substances (Jerlov, 1976; Jupp, 1988)]

The material in the water column influences the amount of absorption and scattering of radiation. This effect, which varies with wavelength, is represented by the coefficient of water attenuation (K) and this property is important when considering the effect of depth on the amount of radiation returning to the sensor.

In general, previous workers have attempted to process the data for individual parameters without incorporating other effects in the model. Numerous studies, for example, attempt to individually measure suspended sediment concentration (SSC) (Amos and Alfoldi (1979) and various studies summarized in Curran and Novo (1988)), salinity (Khorram, 1982), and chlorophyll concentration (Gordon *et al.*, 1980; Stumpf and Tyler, 1988). These studies derive empirical relationships between concentration remotely sensed radiance by obtaining simultaneous field measurements. These derived relationships, which exlude the effects of other materials, water depth, and substrate reflectance, are scene specific and, impractically, require ground calibration at the time of overpass.

Substrate enhancement algorithms are generally rare. A useful method is that of Lyzenga (1981) which produces a single index value of substrate reflectance for each pixel based on the ratio of the logarithm of radiances (x_i/x_j) in two bands. If x_i is plotted against x_j, pixels of the same substrate type should plot on a straight line. If the substrate reflectance changes, the data points will fall on a parallel line. By simple geometry, it is possible to derive an index for substrate spectral variability. The problem is that the single image produced from two bands, while indicating change in bottom type, does not indicate the bottom spectral characteristics. Neither does it derive depth information.

Methods for deriving bathymetry from multispectral data generally incur problems when the substrate reflectance varies appreciably (Nordman *et al.*, 1990; Jupp, 1988). The multiple band method of Nordman *et al.* (1990) requires the regression of known depth points against the logarithm of

*Presented at the First Thematic Conference on Remote Sensing for Marine and Coastal Environments, New Orleans, Louisiana, 15-17 June 1992.

P. N. Bierwirth, T. J. Lee, and **R. V. Burne**
Australian Geological Survey Organisation, Environmental Geoscience & Groundwater Program, P. O. Box 378, Canberra, ACT, Australia

Photogrammetric Engineering & Remote Sensing, Vol. 59, No. 3, March 1993, pp. 331–338.

0099-1112/93/5903–331$03.00/00

Landsat TM radiance values to determine scene coefficients. This requires available bathymetric data for each scene to be processed. Although coefficients and water depths are determined separately for various pre determined categories of substrate, misclassifications and substrate variations within these zones will induce depth errors. The depth of penetration (DOP) algorithm of Jupp (1988) is a step determination of depth zones based on a depth of penetration threshold for each band. Threshold values are determined from the maximum deep-water radiances, and for Landsat TM only six water depth zones or depth values can be derived. Although in some areas dark substrates such as sea-grasses may be misinterpreted as deep water, the technique is probably the most reliable for use in navigation. Jupp (1988) discusses ways of interpolating depth and broadly classifying substrate types within zones, although the variation of both of these factors may confuse the result.

In this paper, we take a different approach by deriving both substrate reflectance and depth from the same algorithm. The aim is to derive substrate reflectance factors in each band processed and, as a by-product, produce a continuous grey-scale depth image. At this stage of our research, we assume relatively clear water and only minor variations in the concentration of water column materials.

Theory

Light entering a water column is subjected to absorption and scattering from both the water-body and the substrate (Figure 1). The attenuation of light energy, increasing with depth, due to light absorption by water molecules, dissolved substances or particles (both organic and inorganic) and due to scattering from suspended particles, may be described by Equation 1 below.

$$T_r = e^{-\alpha z} \tag{1}$$

Here T_r is the fraction of the radiant flux at a depth z compared to the incident radiant flux, and α is the volume attenuation constant assuming a homogeneous medium (Jerlov, 1976). Jupp (1988) has given a more generalized version of this formula shown by Equation 2, to allow for the effects of the substrate reflectance.

$$L_E = (e^{-2kz})L_b + (1 - e^{-2kz})L_w \tag{2}$$

Here L_E is the radiance emerging from the water mass, L_b is the radiance of (wet) substrate material for no water cover (*i.e., for* $z = 0$), L_w is the radiance of deep water, and k is the effective attenuation coefficient for the water-body.

It is preferable to look at reflectance properties rather than radiance because reflectance, of substrate and water column materials, is a measurable quantity independant of illumination conditions. Because reflectance is the ratio of emergent radiance relative to the total irradiance, it follows that reflectance is proportional to radiance. This means that the water radiance equation of Jupp (1988) (Equation 2) can be normalized to reflectance; i.e.,

$$R_E = (e^{-2kz})R_b + (1 - e^{-2kz})R_w \tag{3}$$

Method

In what follows, it will be assumed that the water column reflectance, R_w, due principally to suspended sediments and organic matter, remains constant over the scene. Before attempting to unmix substrate reflectance and depth parameters, the raw sensor count values or digital numbers (DNs) need to be converted to a term which estimates reflectance.

Conversion of Sensor DN to Reflectance Estimates

In practice, many other effects influence the amount of radiation recorded at the satellite or aircraft sensor (Figure 1). This figure shows that light emerging from the water mass is also influenced by the atmosphere. The radiance transmitted by the atmosphere can be given by

$$L_T = (L_E + L_{ws})T_\phi = (R_E + R_{ws})T_\phi I. \tag{4}$$

Here L_{ws} is the radiance from the water surface and all other symbols are defined below Figure 1. The total solar irradiance, I, just above the water surface is described by Equation 5 (see Richards, 1986); i.e.,

$$I = E_0 T_\theta \cos\theta + E_D \tag{5}$$

Here T_θ is the transmittance of the solar irradiance, E_0 and the $\cos\theta$ term arises because we are interested in the vertical component of the incident light energy. These factors determine the amount of direct solar irradiance which is added to the diffuse sky irradiance before being reflected. The radiance received at the sensor, L_S, is the sum of the radiance directly transmitted from the target, L_T and the radiance due to atmospheric back-scatter, L_P. Pixel radiance can be related to the count value, C(i.e.,DN), by Equation 6 below.

$$L_S = L_T + L_P = CG + L_{\min} \tag{6}$$

Here G is the instrument gain and $L_{\min}$ is the instrument

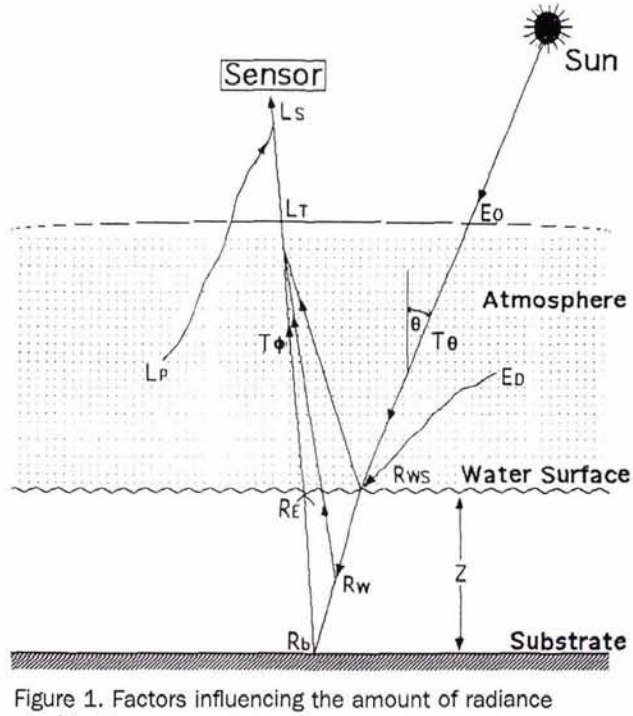

Figure 1. Factors influencing the amount of radiance reaching a sensor over a water mass.

E_o	solar illumination at the top of the atmosphere
T_ϕ,T_θ	atmospheric transmittance
E_D	diffuse sky irradiance
R_{ws}	reflectance from the water surface
R_w	reflectance from molecules and particles in the water column
R_b	substrate reflectance
R_E	effective reflectance of the water body (not including R_{ws})
L_P	atmospheric path radiance (back-scatter)
L_T	radiance from the target transmitted by the atmosphere
L_S	radiance received at the sensor

offset. Combining Equation 4 and 6 creates Equation 7 which relates C to the reflectance, R_E, the standard quantity that we wish to examine more closely for substrate effects.

$$C = R_E(IT_\phi/G) + R_{ws}(IT_\phi/G) + (L_P - L_{min})/G. \quad (7)$$

Generally, the factors can be split into additive and multiplicative influences on the water mass reflectance to make up the recorded signal. Raw Landsat pixel DN values are corrected to estimate the true reflectance in two stages by successively removing these additive and multiplicative effects.

First, minimum value statistics for each band are collected for the scene. It is assumed that the lowest count value for a pixel is located where the water is relatively clear and deep, i.e., where L_E is approximately equal to L_w. The radiance emerging from the water mass will be small, and the lowest value will represent all the additive components if we assume that the path radiance L_P and T_ϕ (measuring atmospheric absorption) remain constant for a particular band over the scene. Therefore, $C = C_{min}$ and

$$C_{min} = R_{ws}(IT_\phi/G) + (L_P - L_{min})/G. \quad (8)$$

Substracting C_{min} from every raw pixel DN gives

$$C_1 = C - C_{min} = R_E IT_\phi/G. \quad (9)$$

Second, values for the instrument gain, G, and average solar irradiances, I, for the Landsat 5 sensor are found from the Landsat technical notes (Markham and Barker, 1986) and are used to further correct the data by means of Equation 10; i.e.,

$$C_2 = C_1 G/I = R_E T_\phi. \quad (10)$$

The corrected pixel value C_2 estimates the reflectance term. Variations from true reflectance will mainly be due to atmospheric absorption and will increase toward the shorter wavelengths in a Rayleigh-type atmosphere (Forster, 1984). It should be noted here that the second stage correction for multiplicative effects is not absolutely necessary for deriving substrate parameters, although there are certain advantages. This will be discussed later.

For the situation where the estimate for C_{min} is valid, the effect of the subtraction in Equation 9 is to remove the major additive component (i.e., atmospheric back-scatter, L_P) and all but eliminate the effects of deep water radiance, L_w (see Equation 3).

Unmixing Substrate Reflectance and Depth Parameters

From Equation 3, the reflectance equation becomes

$$R_{Ei} - R_{wi} = R_i = R_{bi}e^{-2k_i z}; \qquad i = 1,N. \quad (11)$$

The subscript i specifies the wavelength (band) for each equation and N is the number of such bands. R_i represents the reflectance-corrected Landsat data. Equation 11 is a convenient base from which a to describe our method for unmixing the effects of substrate reflectance, R_{bi}, from those of depth, z.

Taking the logarithm of both sides of Equation 11 gives

$$\ln(R_i) = \ln(R_{bi}) - 2k_i z; \qquad i = 1,N. \quad (12)$$

In this set of equations where the depth is unknown and constant, the substrate reflectances R_{bi} are also unknown and vary. Assuming that the corrected sensor values approximate the water mass reflectances, R_i and that the water attenuation coefficients, k_i, can be derived, there are still N equations with $N+1$ unknowns. Therefore, it is not possible to obtain a unique solution, yet a strategy is needed to map the multispectral features of the substrate independent of depth effects.

Summing Equation 12 over N bands gives and equation for the water depth:

$$z = \sum_{i=1}^{N} \frac{\ln R_i}{(-2k_i N)} - \sum_{i=1}^{N} \frac{\ln R_{bi}}{(-2k_i N)}. \quad (13)$$

The aim is to unmix or solve for the substrate reflectances or a factor representing R_{bi} which is invariant with changes in water depth. This can be achieved by setting the constraint:

$$\sum_{i=1}^{N} \frac{\ln R_{bi}}{(-2k_i N)} = M \quad (14)$$

where M is an arbitrary constant which standardizes the geometric mean of substrate reflectance for every pixel. Because reflectance is between 0 and 1, the value of M will, in a true sense, be positive and tend toward zero at 100 percent reflectance (i.e., $R_{bj}=1$). We choose to set $M=0$ for reasons of convenience as explained later.

Combining Equations 13 and 14 provides an estimate (Z) of the true depth (z):

$$Z = \sum_{i=1}^{N} \frac{\ln R_i}{(-2k_i N)} - M = \sum_{i=1}^{N} \frac{\ln R_i}{(-2k_i N)}. \quad (15)$$

Substituting this value into Equation 11 gives a solution for substrate reflectance:

$$R_{Bi} = R_i e(2k_i Z); \qquad i = 1,N. \quad (16)$$

where R_{Bi} is the derived estimate of true substrate reflectance (R_{bi}). The values for Z and R_{Bi} are algorithm outputs which can be displayed as images by scaling the numbers into the byte (0 to 255) range.

By setting $M=0$, the geometric mean of substrate reflectance is forced to equal one, which effectively brightens the substrate over all bands. The effect of the constraint may be viewed as inducing an error, Δz, in the depth (i.e., $\Delta z = Z - z$) which, conveniently if $M=0$, will always be positive. From Equation 16 it can be seen that

$$R_i = R_{Bi}e^{-2k_i Z} = (R_{bi}e^{2k_i \Delta z})e^{-2k_i(z+\Delta z)} \quad (17)$$

and the estimate substrate reflectance (R_{Bi}) can be represented in terms of the true reflectance (R_{bi}) by

$$R_{Bi} = (R_{bi}e^{2k_i \Delta z}). \quad (18)$$

There is a problem here because variations in Δz will alter the intra-band (spectral) relationship or hue, as a consequence of differing values of k_i. This means that the colors of the imaged substrate reflectance may change with variations in depth or substrate albedo. However, this may be overcome by using the quantity $R_{Bi}^{(1/2k_i)}$ so that

$$R_{Bi}^{(1/2k_i)} = R_{bi}^{(1/2k_i)}e^{\Delta z}. \quad (19)$$

The true reflectance properties will then be scaled by the same constant for each band which varies between pixels. This means that the spectral hue of the substrate will be preserved regardless of depth variations. This then represents the substrate enhancement that we set out to achieve.

Application of the Method

The approach has been tested using data from Hamelin Pool, Shark Bay, Western Australia (Figure 2). The area was selected because (1) it is characterized by shallow, clear waters of oceanic derivation; (2) detailed bathymetric data are available; (3) there are contrasting bottom types within each depth range; and (4) considerable research has been undertaken on the benthic ecology and sediment types (Logan

and Cebulski, 1970; Hagan and Logan, 1974; Burne and Hunt, 1990).

The data-sets used were a Landsat 5 TM multispectral image WRS 115–076 captured on 30 August 1986 (30-m pixel resolution) and precise bathymetric data acquired in the form of well located and closely spaced hydrographic soundings by the Australian Survey Office, restored to Australian Height datum and gridded as a raster image with a 50-m pixel resolution.

As the water attenuation, k_i, increases with longer wavelengths, the signal (R_i) becomes very small and immersed in sensor noise for deeper waters. Therefore, it was decided to use only the first three bands of the Landsat TM in which reasonable water penetration can be achieved (see Table 1).

A certain amount of processing of the data was required before analysis.

First, to enable direct comparison between the bathymetric information derived from analysis of the satellite data and that produced by the hydrographic survey, the Landsat TM data were registered (image to image) to the bathymetry (registered to AMG) and resampled to 50 m using billinear interpolation and a second-order polynominal (Richards, 1986). Plate 1a shows the resampled TM bands 1, 2, and 3 as red, green, and blue, respectively, and Figure 3 shows the gridded grey-scale bathymetry. Comparison of these figures reveals several dark features in Plate 1a which do not correspond to deeper water areas in Figure 3. Notable examples are the dark area in the southern part of Hamelin Pool which corresponds to an area of benthic organic ooze that is mainly composed of diatoms (Burne and Hunt, 1990) and the bluish area in the northeast corner of the image which corresponds to the southern part of the Wooramel Sea-grass Bank (Logan and Cebulski, 1970; Davis, 1970). It is important to note that, apart from this area of sea grass, substrate colors are subdued in the raw data due to the dominating contrast effects of water depth variations. It is precisely this effect that this analysis is designed to remove.

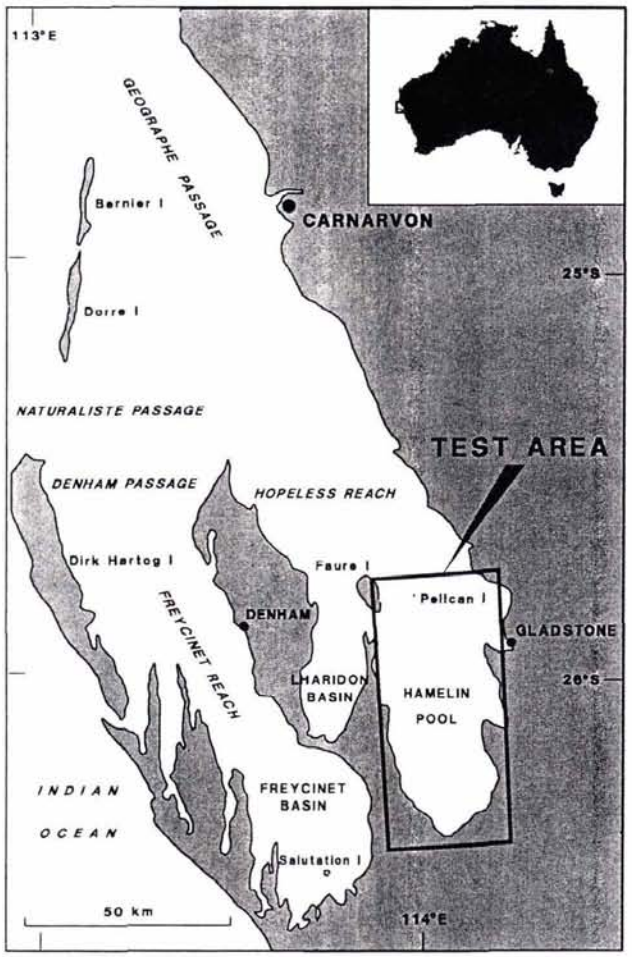

Figure 2. Location map for test area.

Second, Lansat TM bands 1, 2, and 3 were converted to estimate reflectance by the two calibration stages described earlier.

Finally, it was necessary to determine reasonable values for water attenuation and coefficients (k) to Landsat TM bands 1, 2, and 3. For clear water of the type found in Hamelin Pool, values for k should increase for longer wavelengths in the range recorded by Landsat TM (Jerlov, 1976). The co-registered bathymetry and Landsat data were used together with Equation 12 to derive these values. Sub-areas were chosen where substrate type remained relatively constant but depth varied. If these conditions are true, scattergrams of the logarithm of pixel reflectance (R_i, derived from Landsat) versus depth (z, drived from bathymetry) should show a cloud of data with a well-defined axis (see Figure 4). Figure 4 shows that the sub-area chosen is adequate in that substrate reflectance remains relatively constant for each band because the data cloud is strongly elongated. The slope of the regression line through the data represents the quantity, $-2k_i$, (see Equation 12) and the ks determined were $k_1 = 0.100$, $k_2 = 0.130$ and $k_3 = 0.194$ m^{-1}.

Values of k are specific to the unit of depth (metres in this case) and are independent of atmospheric absorption or scaling effects on R_i (see Equation 12). This means that the values of k can be used for other Landsat TM scenes assuming that water column conditions are similar. Given that the Shark Bay waters are hypersaline (salinity just north of Hamelin Pool is about 49°/00 and increased to 65°/00 at the southern end of the Pool) the determined ks may not be appropriate for other scenes. In this case, consideration should be given to alternate approximation methods for water attenuation derivation (e.g., Lyzenga, 1981).

Having found suitable values for k_i in each band, these values, together with the corrected Landsat pixel values, were inserted into Equation 16 to estimate bottom reflectance (Plate 1b). Reflectance values were scaled for display so that 0 and the maximum R_{Bi} equaled 0 and 255, respectively. In this image colors are independent of depth. Sea grasses and microbial mats show as cyan to blue whereas sandy areas show as red to yellow.

Because chlorophyll absorbs strongly in band 1 (Gordon *et al.*, 1980), the ratios of substrate reflectance R_{b2}/R_{b1} and R_{b3}/R_{b1} are effective enhancements for the presence of chlorophyll. We present the latter ratio (see Figure 5) which appears to give slightly better definition. Sea-grass areas show brightly in the northeast and are partly associated with tidal channels. Also, microbial mats are bright around the edges of

TABLE 1. ANALYSED LANDSAT TM WAVELENGTHS

Band	Wavelength (nm)
1	450–520
2	520–600
3	630–690

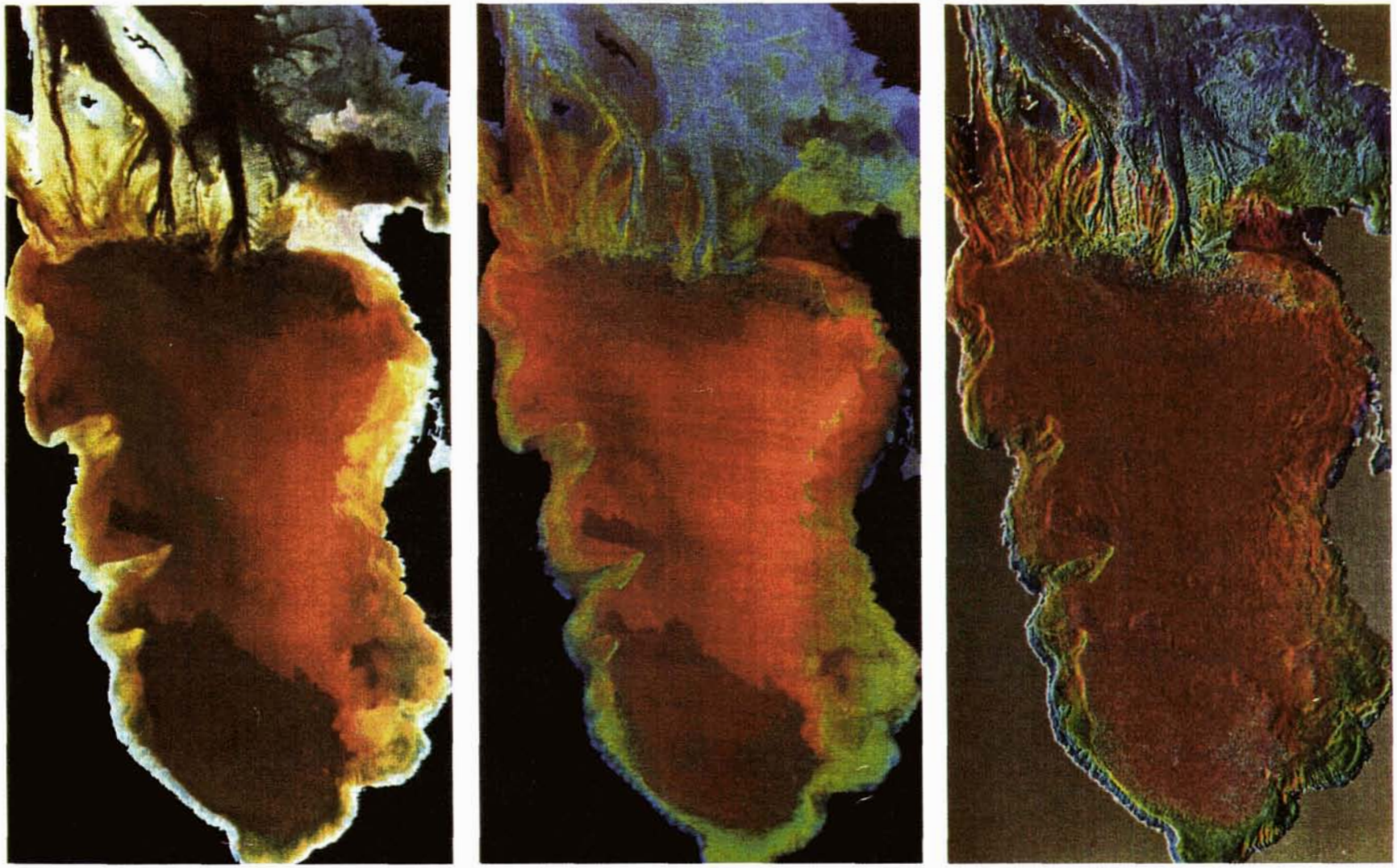

(a) (b) (c)

Plate 1. (a) Landsat TM bands 1, 2, and 3 shown in red, green, and blue, respectively. Land is blacked out. (b) Algorithm derived substrate reflectance bands 1, 2, and 3 shown in red, green, and blue, respectively. This is a residual image after the removal of depth. (c) Satellite derived substrate reflectance and depth combined using the HSI procedure. The hillshaded depth image is substituted for the intensity of the substrate image (image b).

Figure 3. Hydrographic survey bathymetry for Hamelin Pool. Depth soundings were scaled so that 11 metres equaled a display DN of 255.

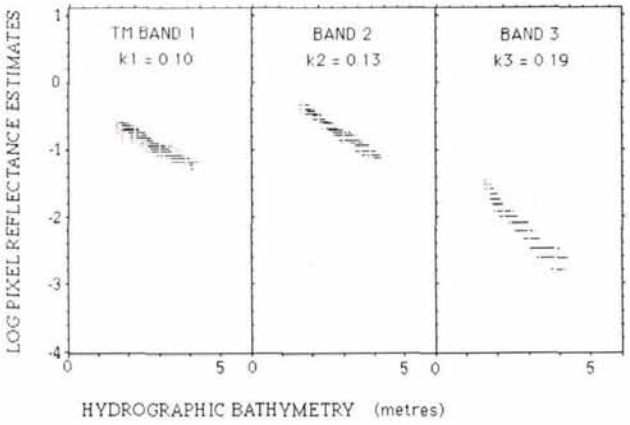

Figure 4. Attenuation coefficient determinations from subscene scattergrams for Landsat TM bands 1, 2, and 3 plotting the logarithm of pixel reflectance versus depth.

Hamelin pool. Some chlorophyll is also detected in the area of organic ooze (bottom center of pool).

Figure 6 shows the depth image (compare with Figure 3) derived from the TM data using Equation 15. The satellite-derived depth image (Figure 6) shows errors at the bottom of the image due to a dark substrate (as previously discussed) associated with the area of organic ooze. Depth may also be exaggerated in the main tidal channel due to the presence of sea grass. Problem areas such as these can be identified in the bottom-reflectance image (Plate 1b) as having a significant relative blue component.

Pixel values for hydrographic bathymetry (shown in figure 3) (true) were plotted against co-registered algorithm-derived Landsat TM water depths (derived) (see Figure 7). As a summary of statistical correlation between the data-sets, a regression analysis was performed and the results are shown in Table 2.

The linear correlation coefficient shows a reasonable linear correlation between "true" hydrographic bathymetric soundings and estimated water depth derived from Landsat TM data. The intercept indicates the average error in depth estimation, Δz, at very shallow depths and may show the influence of band gain factors which were not completely removed in the initial correction of raw DNs to reflectance. The slope value is small compared with a slope of unity for a perfect correlation. The most likely explanation for this is that the water attenuation coefficient, k_i, decreased in deeper water. This is consistent with earlier observations (Jerlov, 1976) of variable k's with depth due to the gradation of decaying organic matter to lower concentrations at depth.

Detailed structure can be viewed in the depth image (Figure 6) by applying artificial illumination. Figure 8 was derived using a hillshade algorithm with an illumination source at 100° azimuth and 30° elevation. An intricate pattern of tidal channels and ridges can be seen on the Fauré Barrier Bank toward the top of the image (see Figures 35, 36, and 37 of Hagan and Logan (1974)).

Figure 5. Chlorophyll enhancement. Scaled ratio of substrate reflectance band3/band1.

Figure 6. Estimated water depth derived from Equation 15 and Landsat TM bands 1, 2, and 3.

A useful way of combining the substrate-reflectance and depth images is to transform the substrate-reflectance data to hue, H, saturation, S, and intensity, I (Gillespie *et al.*, 1986). The intensity is then replaced by hillshaded depth and the data transformed from HSI back to RGB color space (Plate 1c).

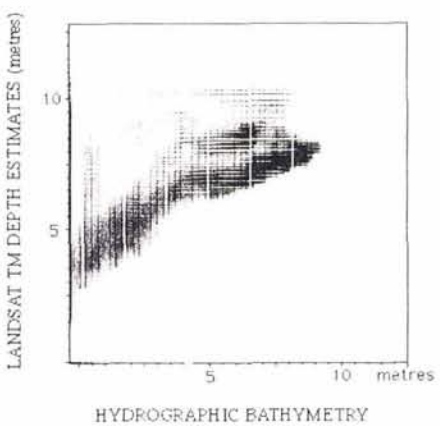

Figure 7. Scattergram plotting hydrographic bathymetry versus Landsat TM derived water depth.

TABLE 2. REGRESSION ANALYSIS STATISTICS RELATING TO FIGURE 7

N (number of samples)	480047
Linear correlation coefficient	0.7849555
Multiple R - Square	0.6149
Intercept	4.5785 (std. err. = 0.0033)
Slope	0.4482 (std. err. = 0.0005)

Colors of the substrate-reflectance are preserved, but the intensity shows the structure of the depth image.

The estimate of water depth and substrate composition also allows three-dimensional viewing of the sea floor. By inverting depth to give elevation data, 3D perspectives are obtainable (Bierwirth *et al.*, 1992). Steroscope viewing is also effective using stereo pairs generated from the inverted depth and substrate reflectance images.

Discussion

The modeling described here represents a new method for processing multispectral data to derive substrate color, structure, and depth information. The method was successfully tested in the Hamelin Pool area of Shark Bay, Western Australia. Although most effective in areas of clear water such as this, it should also be readily applicable to other coastal regions. As such, the process represents a valuable tool for the analysis and management of coastal zones.

It is important to note that, in applying the constraint which standardizes the sum of the logarithms of band substrate reflectances, we introduce errors in depth determina-

Figure 8. Hill-shaded satellite derived depth. Illumination source at 100° azimuth and 30° elevation.

tions. These errors are greatest for dark substrates which will resolve as deeper than true.

As mentioned previously, the corrections for illumination, sensor, and atmospheric gains are not essential when only relative substrate reflectances are required. It can be demonstrated that the effect of signal multiplying influences will result in a band-constant scaling of substrate reflectances, and this effect is removed when scaling values for display purposes. If, however, standard values of substrate reflectance or depth are required for multidate scene comparisons, gain corrections may be necessary. This is because estimated depths will contain a constant additive factor and substrate reflectances will be multiplied by a factor, both related to the gains.

The advantage of the method described by this paper is the derivation of substrate-reflectance parameters, for each band, which define standard properties of bottom materials over the scene, free from the confusing effects of depth variation. In Hamelin Pool, features obscured by the depth effect in the raw data, such as sea-grasses in dark tidal channels and microbial mats in the highly reflective sub-littoral zone, were clearly distinguished in the substrate enhancement (see Plate 1b). Substrate reflectance images derived by the method therefore represent the optimum enhancement which can be used as a basis for substrate classification.

In this study, water attenuation coefficients were determined by regressing known bathymetric data against Landsat radiances. Because bathymetric data are not commonly available in many areas, it is proposed that the coefficients derived for the Shark Bay area be tested in the processing of other scenes. However, considering that the waters of Hamelin Pool are unusual in that they are free of suspended sediment, low in nutrients and phytoplankton, and are hypersaline, this proposal may not be valid. More work needs to be done, therefore, both in measuring water attentuation coefficients for various waters and in developing alternative methods for deriving k_i from the data.

Water attenuation may vary also within a scene due to changing concentrations of water column materials. In this work, water column conditions were assumed to be constant over the scene. Although this may be a reasonable assumption in the relatively clear waters of Shark Bay, it is unlikely to be true in many other coastal regions where variations in suspended sediment (SSC), for example, is an important factor. In future work, the effects of water column parameters need to be incorporated within the context of a global mode. This might be achieved by utilizing multispectral scanners with high spectral resolution where visible and near-infrared bands could be used to separate substrate and water-column parameters.

In conclusion, the method presented here is new and represents a significant development for substrate mapping using multispectral data. The important aspect is that the confusing effect of water depth variation is removed, leaving, as a residual, the spectral nature of the substrate. This facilitates improved accuracy in the remote mapping and monitoring of the aquatic environment.

Acknowledgements

The authors wish to knowledge the Australian Survey Office for the acquisition and provision of depth sounding data. Within the Australian Geological Survey we wish to thank both Phil McFadden and Colin Simpson for their comments and also Evert Bleys for his contribution to manuscript preparation.

References

Amos, T. T. and C. L. Alfoldi, 1979. The determination of suspended sediment concentration in a macrotidal system using Landsat data. *Journal of Sedimentary Petrology*, 49 (1): 159-174.

Bierwirth, P.N., T. J. Lee, and R. V. Burne, 1992. Shallow water mapping via the separation of depth and substrate components from multispectral data: an example from Useless Inlet, Shark Bay, Western Australia. *Proceedings of the Sixth Australian Remote Sensing Conference*, Wellington, New Zealand. 1: 99-109.

Burne, R. V., and G. Hunt, 1990. The geobiology of Hamelin Pool: Research reports of the Baas Becking Geobiological Laboratory's Shark Bay Project. *BMR Geology and Geophysics, Australia, Record 1990/89*, 288 p.

Curran, P. J., E. M. M. Novo, P. J., and E. M. M. Novo, 1988. The relationship between suspended sediment concentration and remotely sensed spectral radiance. *Journal of Coastal Research*, 4(3): 351-368.

Davies, G. R., 1970. Carbonate bank sedimentation, eastern Shark Bay, Western Australia. *American Association of Petroleum Geologists Memoir*, 13: 85-168.

Forster, B. C., 1984. Derivation of atmospheric correction procedures for LANDSAT MSS with particular reference to urban data. *International Journal of Remote Sensing*, 5(5): 799-817.

Gillespie, A. R., A. B. Kahle, and R. E. Walker, 1986. Color enhancement of highly correlated images. 1. Decorrelation and HSI contrast stretches. *Remote Sensing of Environment*, 20: 209-235.

Gordon, H. R., D. K. Clark, J. L. Mueller, and W. A. Hovis, 1980. Phytoplankton pigments from the Nimbus-7 Coastal Zone Color Scanner: comparisons with surface measurements. *Science*, 210(3): 63-66.

Hagan, G. M., and Logan, B. W., (1974). Development of carbonate banks and hypersaline basins, Shark Bay, Western Australia. *American Association of Petroleum Geologists Memoir*, 22:p.61-139.

Jerlov, N. G., 1976. *Marine Optics*, Elsevier, Amsterdam.

Jupp, D. L. B., 1988. Background and extensions to Depth of Penetration (DOP) mapping in shallow coastal waters. *Symposium on Remote Sensing of the Coastal Zone*. Gold Coast, Queensland, Session 4, Paper 2.

Khorram, S., 1982. Remote sensing of salinity in the San Francisco Bay delta. *Remote Sensing of Environment*, 12: 15-22.

Logan B. W., and D. E. Cebulski, 1970. Sedimentary environments of Shark Bay.. Australia. *American Association of Petroleum Geologists Memoir*, 13: 1-37.

Lyzenga, D. R., 1981. Remote sensing of bottom reflectance and water attenuation parameters in shallow water using aircraft and Landsat data. *International Journal of Remote Sensing*, 2(1) 71-82.

Markham, B. L., and J. L. Barker, 1986. Landsat MSS and TM post-calibration dynamic ranges, exoatmospheric reflectance and at-satellite temperatures, *Landsat Technical Notes*, Eosat, Lanham, Maryland, August, p. 2-7.

Nordman, M. E., L. Wood, J. L. Michalek, and J. L. Christy, 1990. Water depth extraction from Landsat-5 imagery. *Proceedings of the Twenty-Third International Symposium on Remote Sensing of Environment*, pp. 1129-1139.

Richards, J. A., 1986. *Remote Sensing Digital Image Analysis: An Introduction*. Springer-Verlag, Berlin.

Smith, R. C., and K. S. Baker, 1981. Optical properties of the clearest natural waters (200-800) nm. *Applied Optics*, 20(2): 177-184.

Stumpf, R. P., and M. A. Tyler, 1988. Satellite detection of bloom and pigment distributions in estuaries. *Remote Sensing of the Environment*, 24: 385-404.